

Supporting information

Chemical Tuning of Coulomb Blockade at Room-Temperature in Ultra-Small Platinum Nanoparticle Self-Assemblies

Simon Tricard,^{a*} Olivier Saïd-Aïzpuru,^a Donia Bouzouita,^a Suhail Usmani,^a Angélique Gillet,^a Marine Tassé,^b Romuald Poteau,^a Guillaume Viau,^a Phillipe Demont,^c Julian Carrey,^a and Bruno Chaudret^{a*}

^a *LPCNO, INSA, CNRS, Université de Toulouse, 135 avenue de Rangueil, 31077 Toulouse, France*

^b *LCC, CNRS, Université de Toulouse, 205 route de Narbonne, 31077 Toulouse, France*

^c *Institut Carnot – CIRIMAT, Université de Toulouse, 118 route de Narbonne, Toulouse, France*

* *Corresponding authors: tricard@insa-toulouse.fr; chaudret@insa-toulouse.fr*

Content: statement of contributions, experimental methods, references for DFT calculations, discussion on axial vs. global polarizability, supplementary characterizations, and experimental values.

Statement of contributions: ST, OSA, DB and AG performed the experimental syntheses and characterizations; ST, OSA and MT performed the charge transport measurements by conductive AFM; SU and JC performed the charge transport measurements by the interdigitated combs technique; PD performed the charge transport measurements by dielectric spectroscopy; ST and GV performed the X-Ray diffraction measurements; RP performed the theoretical calculations; ST and BC supervised the project and wrote the manuscript. All authors discussed the results and commented on the manuscript.

Experimental methods

Chemical synthesis

Synthesis of the nanoparticles. All operations were carried out using Fischer-Porter bottle techniques under argon. A solution of $\text{Pt}_2(\text{dba})_3$ (90 mg; 0.165 mmol of Pt) in 20 mL of freshly distilled and deoxygenated THF was pressurized in a Fischer-Porter bottle with 1 bar of CO during 30 minutes at room temperature under vigorous stirring. During this time, the solution color changed from violet to brown (attesting the formation of the nanoparticles). The mixture was evaporated and washed with pentane to eliminate the dba (3 x 20 mL), and to obtain native nanoparticles. The colloid was then redissolved in 20 mL of THF. The size of the nanoparticles can be controlled at this step, by letting them ripening under agitation at room temperature. The size evolves with time: directly after the synthesis: 1.1 nm, after 15 hours: 1.7 nm. Intermediate sizes are obtained for intermediate ripening time, and larger sizes for longer time (up to 2.0 nm after four days). For each series of measurements, the sizes were determined by TEM imaging.

Assembly of the nanoparticles. 1 mL of a solution of the thiol ligand (between 0.1 eq. and 0.4 eq. per introduced Pt) was added to 4 mL of the native nanoparticle mixture. The brown solution was agitated for 2 hours. Drops of the crude solution were deposited on specific substrates for each characterization (see below). The remaining solution was evaporated to dryness and was isolated as dark-brown powder.

[Assemblies are formed either in rod or platelet shapes; there is no trivial explanation to why/how these anisotropic structures form, starting from isotropic building blocks, and without showing any supra-particular order. Current investigations are carried out in our laboratory to solve this question.]

Structural characterization of the assemblies

Samples for TEM were prepared by deposition of one drop of the crude solution on a carbon covered holey copper grid. TEM analyses were performed at the “centre de microcaractérisation Raimond Castaing” using a JEOL JEM 1400 electron microscope operating at 120 kV. The mean size of the particles was determined by image analysis on a large number of particles (~300) using the ImageJ software.

FT-IR spectra were recorded on a Thermo Scientific Nicolet 6700 FT-IR spectrometer in the range 4000-700 cm^{-1} , using a Smart Orbit ATR platform. The sample deposition was performed by drop casting of the crude solution on the germanium crystal of the platform; the measurement was acquired after evaporation of the THF solvent.

X-ray diffraction patterns were recorded on a PANalytical Empyrean diffractometer using the Co K α radiation. Wide angle measurements were realized on powder. The line broadening (full width at half-height) was measured using the Highscore software. The crystallite size was inferred from the line broadening using the Scherrer formula. Small angle measurements were performed on a microscopy glass, on which the crude solution was drop casted. An advantage of working with particles smaller than 2 nm is that the inter-particle distance is sufficiently small to observe correlation distances between two particles with a regular XRD diffractometer without the need of any dedicated SAXS facilities.

Charge transport measurement with the interdigitated combs device

The electrodes for the transport measurements consisted of eight pairs of interdigitated combs elaborated by photolithography^{15,18}. They were composed of 20 interpenetrated fingers with a height of 30 nm, a length of 200 μm , and separated by a gap of 5 μm . Integration of the particles between the electrodes was performed by dielectrophoresis. To do so, a droplet a colloidal solution was deposited on the sample while an ac voltage of 7.6 V rms at 10 kHz was applied to the electrodes. After 20s, the droplet was dried using a paper. Transport measurements were performed in a nitrogen-cooled cryostat using a Keithley 6430 sub-femtoamperemeter.

Charge transport measurement by conductive-AFM

Measurement. Conductive AFM measurements were performed with an AIST-NT SmartSPM 1000 microscope, equipped with a conductive AFM unit. The samples were prepared by drop casting of one drop of the crude solution on silicon wafers covered by a \sim 50 nm layer of gold (with a \sim 5 nm chromium anchoring layer). We always used conductive silicon tips covered by platinum (Mikromash HQ-NSC15/Pt), but we double-checked that similar behaviors were observed with doped-diamond coated tips (NT-MDT DCP10), to confirm that the trends did not come from contact effects. Typical measurements consisted in first performing a topography image of the sample and then going in contact on zones with individual assemblies to measure their I - V characteristics. Measurements were performed on several objects per zone and several zones of the substrates.

Data analysis. The I - V characteristics were normalized at 2 V for the aryl series and at 5V for the alkyl series. We then averaged the characteristics on 50 curves (error bars on the graphs are 95% confidence intervals). In order to fit the $I \sim V^{\xi}$ behavior, the linear component determined at low I values was subtracted and data were fitted for positive I values by the formula $I/I(2V) = (V/2)^{\xi}$ for the aryl series and by the formula $I/I(5V) = (V/5)^{\xi}$ for the aryl series. The charging energies were calculated by the formula

given in the main text; all the experimental data necessary to calculate the charging energies are available in Supplementary Tables 1, 2 and 3.

Justification of the fitting choice. We have deliberately chosen not to use any threshold voltage V_C as we think this description does not apply to our system (like in Moreira, H.; Yu, Q.; Nadal, B.; Bresson, B.; Rosticher, M.; Lequeux, N.; Zimmers, A.; Aubin, H. Physical Review Letters 2011, 107, 176803.). As a confirmation we fitted the data measured at the nanoscale as $I \sim (V - V_T)^\xi$, where V_T is the threshold voltage (see table below), and we found almost the same ξ values as for $I \sim V^\xi$, with very small V_T values. The two only times we found non negligible (but small) V_T values were for the 1.7 nm-NPs with HSPhOH and HSPhNH₂, where the curves was the closest to linearity, thus showing the smallest Coulomb blockade. V_T is thus not a correct parameter to describe our system. That is why we preferred to stick with the value of ξ as a descriptive parameter.

Ligand	Nanoparticle size	Fit as $I \sim (V - V_T)^\xi$		Fit as $I \sim V^\xi$
		ξ	V_T	ξ
HSPhOH	1.7 nm	1.97	0.19	2.26
HSPhOH	1.2 nm	2.66	3.4e-4	2.66
HSPhCOOH	1.7 nm	2.74	2.3 e-3	2.74
HSPhCOOH	1.2 nm	3.38	7.3 e-4	3.40
HSPhNH ₂	1.7 nm	2.05	0.12	2.23
HSPhNH ₂	1.2 nm	2.39	0.037	2.46
HSC ₇	1.3 nm	3.06	4.8e-6	3.11
HSC ₈	1.3 nm	3.21	7.1e-4	3.29
HSC ₉	1.3 nm	3.23	1.1e-5	3.29
HSC ₁₀	1.3 nm	3.42	5.3e-4	3.44
HSC ₁₁	1.3 nm	3.40	9.3e-4	3.40
HSC ₁₂	1.3 nm	3.36	8.3 e-4	3.43

Dielectric constant and charge transport measurements by dielectric spectroscopy

Dielectric spectroscopy measurements were performed on powder samples compacted between two stainless steel electrodes (diameter 10 mm) in a Teflon sample holder. The thickness of the powder was as small as possible (~400 μ m) to increase the sensitivity of the measurement. Dielectric measurements were carried out as a function of frequency (10^{-2} - 10^6 Hz) and temperature (100 -296 K) using a Novocontrol broadband dielectric spectrometer at an applied AC of 1 V_{rms} . Frequency sweeps were carried out isothermally. The intrinsic dielectric constant of the free aryl ligands was obtained from the real part $\epsilon'(\omega)$ of the complex dielectric permittivity $\epsilon^*(\omega)$ taken at a high frequency of 1MHz. Measurements on the free alkyl ligands was impossible as the experimental setup is not adapted for liquids. The I - V curves for the powder of nanoparticle assemblies were obtained at a frequency of 1 Hz using 100 mV_{rms} step ranging

from 0 to 3 V_{rms} and at different temperatures ranging from 100 to 296 K. Data were fitted by the simple power law $i \propto V^{\xi}$. Similarly to the charge transport measurements by conductive-AFM, the I-V curves measured by dielectric spectroscopy at the macroscopic scale gave an almost null threshold voltage value at room temperature, which did not vary between 300 and 100K.

Theoretical calculations

All molecular calculations have been performed using the Gaussian09 suite of programs.²⁴ Geometry optimizations and subsequent electronic properties calculations have been performed in the gas phase without symmetry constraints. They have been carried out in the framework of density functional theory (DFT), using the B3PW91 hybrid functional and the aug-cc-pVTZ basis set. Recent benchmark studies showed that the aug-cc-pVTZ basis set is the most accurate to calculate molecular dipole moments and polarizabilities and that coupled cluster-singles and doubles (CCSD), second-order Møller-Plesset (MP2) or hybrid density functional theory (DFT) methods, using this basis set, are all able to predict polarizabilities with RMSD errors lower than 2.5 bohr³. However, the high computational cost of CCSD calculations in very large basis sets make this method available for small compounds only. Polarizabilities have been computed using static frequencies. While the aug-cc-pVTZ basis set is expected to provide state-of-the-art values, we further validated its choice by comparing the obtained polarizability with experimental values calculated using the Clausius-Mossotti relation with refractive indexes given in the literature (Supplementary Table 2). The global polarizability is the trace of the polarizability tensor and corresponds to the three-dimensional polarizability of the molecules. The axial polarizability is the component of the polarizability along the long axis of the chain molecule in a *trans* conformation.

References for DFT calculations.

Program

Frisch, M. J., Trucks, G. W., Schlegel, H. B., Scuseria, G. E., Robb, M. A., Cheeseman, J. R., Scalmani, G., Barone, V., Mennucci, B., Petersson, G. A., Nakatsuji, H., Caricato, M., Li, X., Hratchian, H. P., Izmaylov, A. F., Bloino, J., Zheng, G., Sonnenberg, J. L., Hada, M., Ehara, M., Toyota, K., Fukuda, R., Hasegawa, J., Ishida, M., Nakajima, T., Honda, Y., Kitao, O., Nakai, H., Vreven, T., Montgomery, Jr., J. A., Peralta, J. E., Ogliaro, F., Bearpark, M., Heyd, J. J., Brothers, E., Kudin, K. N., Staroverov, V. N., Kobayashi, R., Normand, J., Raghavachari, K., Rendell, A., Burant, J. C., Iyengar, S. S., Tomasi, J., Cossi, M., Rega, N., Millam, J. M., Klene, M., Knox, J. E., Cross, J. B., Bakken, V., Adamo, C., Jaramillo, J., Gomperts, R., Stratmann, R. E., Yazyev, O., Austin, A. J., Cammi, R., Pomelli, C., Ochterski, J. W., Martin, R. L., Morokuma, K., Zakrzewski, V. G., Voth, G. A., Salvador, P., Dannenberg, J. J., Dapprich, S., Daniels, A. D., Farkas, O., Foresman, J. B., Ortiz, J. V., Cioslowski, J., Fox, D. J. *Gaussian 09* (Revision D.01). Gaussian Inc.: Wallingford, CT, 2009.

Functional

(a) Becke, A. D. *J. Chem. Phys.* **98**, 5648-5652 (1993); (b) Burke, K., Perdew, J. P., Wang, Y., *Electronic density functional theory: recent progress and new directions*, chapter Derivation of a Generalized Gradient Approximation: the PW91 Density Functional. Plenum, New-York (1998); (c) Perdew, J. P., *Electronic structure of solids*, chapter Unified Theory of Exchange and Correlation Beyond the Local Density Approximation. Akademie, Berlin (1991); (d) Perdew, J. P., Chevary, J. A., Vosko, J. A., Jackson, K. A., Pederson, M. R., Singh, D. J., Fiolhais, C., *Phys. Rev. B* **46**, 6671-6687 (1992); (e) Perdew, J. P., Chevary, J. A., Vosko, S. H., Jackson, K. A., Pederson, M. R., Singh, D. J., Fiolhais, C., *Phys. Rev. B* **48**, 4978 (1993); (f) Perdew, J. P., Burke, K., Wang, Y., *Phys. Rev. B* **54**, 16533-16539 (1996); (g) Perdew, J. P., Burke, K., Wang, Y., *Phys. Rev. B* **57**, 14999 (1998).

Basis set

(a) Dunning, T. H., *J. Chem. Phys.* **90**, 1007-1023 (1989); (b) Kendall, R. A.; Dunning, T. H., Harrison, R. J., *J. Chem. Phys.*, **96**, 6796-6806 (1992); (c) Woon, D. E., Dunning, T. H., *J. Chem. Phys.* **98**, 1358-1371 (1993).

Discussion on axial vs. global polarizability

The charging energy E_c of the aryl and alkyl series was calculated knowing s (measured by SAXS), d (measured by TEM) and ϵ_r (measured by dielectric spectroscopy for the aryl thiols). The calculation results are summarized in Supplementary Tables 1, 2 and 3. For the alkyl thiols, dielectric spectroscopy measurements were impossible because of their liquid state at room temperature; we thus calculated their polarizability α by density functional theory (DFT), and deduced their dielectric constant ϵ_r with the Clausius-Mossotti relation $\alpha = (\epsilon_r - 1) / (\epsilon_r + 2) * 3M / (4\pi DN_A)$, where N_A is the Avogadro number, M the molar mass, and D the density of the molecules. An advantage of theoretical calculations is the possibility to dissociate the global polarizability (*i.e.* averaged in three dimensions) from the axial polarizability (*i.e.* the component along the axis of the molecules in a *trans* conformation – Supplementary Table 2). A noticeably good correlation was observed between the evolution of the fitted ξ and the calculated charging energies (Fig. 4e). For the alkyl thiols, it was necessary to use the axial polarizability to obtain such a good correlation (Supplementary Fig. 6), demonstrating the crossing of the electrons through the backbone of the molecules and a structuration of the alkyl thiols in a *trans* conformation in the SAs.

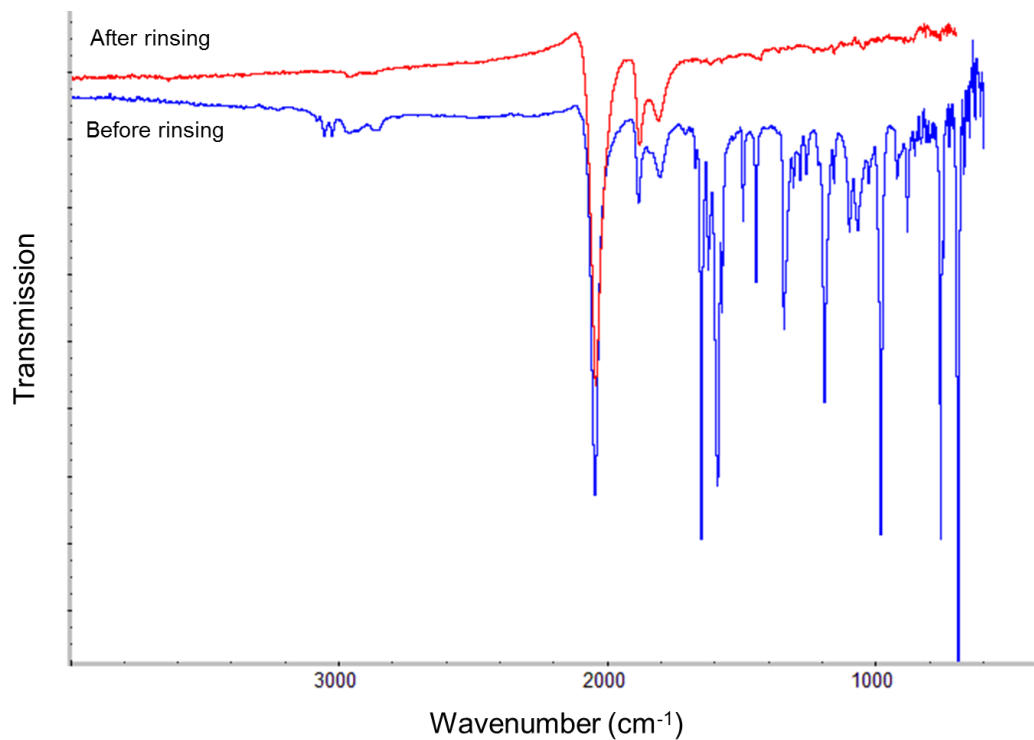


Fig. S1 FT-IR spectra of the starting nanoparticles, before washing (the finger print of the dibenzylideneacetone, dba, is visible in the 800-1850 cm^{-1} region, in addition to the CO stretching bands in the 1850-2100 cm^{-1} region) and after washing (the dba signal is not visible anymore; only the CO signal remains visible). Almost all the dba is removed after washing, the nanoparticles are organic ligand-free, only stabilized by CO and by the coordinating solvent THF.

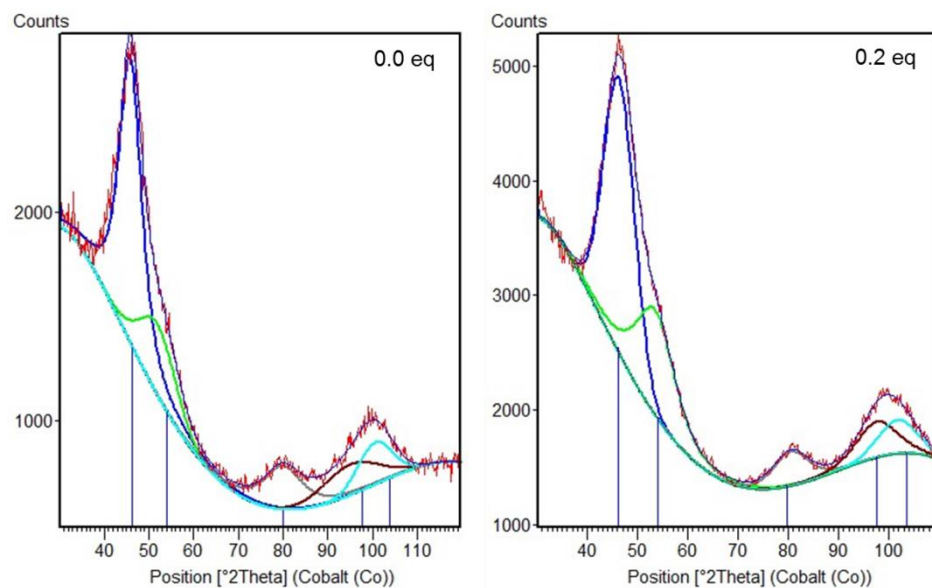


Fig. S2 Wide angle XRD patterns on the native nanoparticles (0.0 eq), and on the assembled particles with 0.2 eq. of HSPhOH. In both samples, the crystalline structure of fcc platinum is found (colored lines are deconvolutions of the (111), (200), (220), (311) and (222) peaks, blue lines correspond to the pdf file n°4-0802), with crystallite sizes of 1.3 nm – given by the Scherrer formula – in the same range as the particle size found by TEM. The platinum particles are thus monocrystalline, and are not subject to crystalline modification during the assembly.

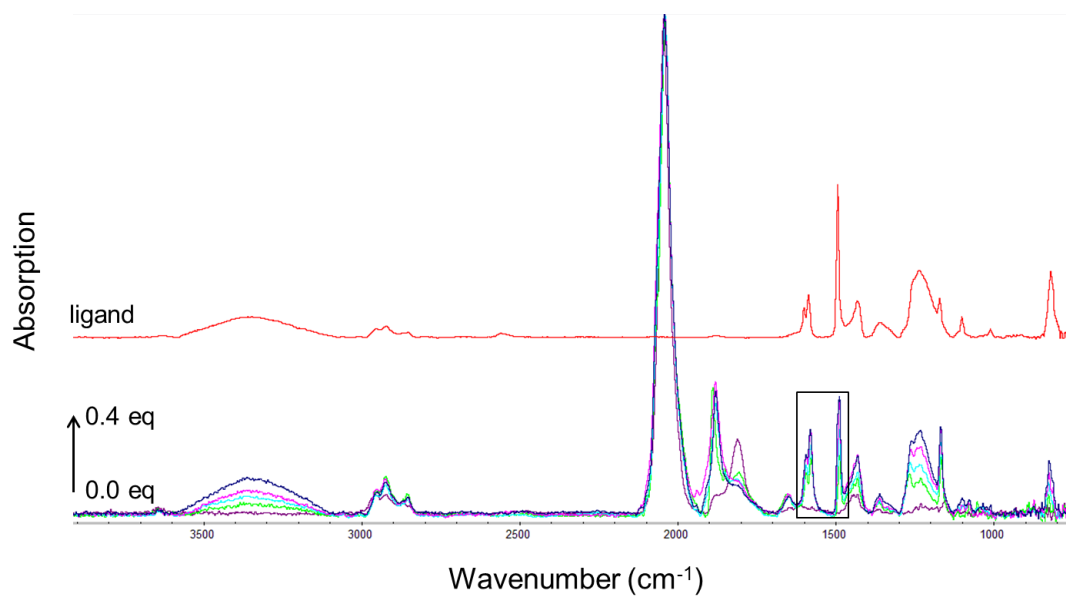


Fig. S3 Full range FT-IR spectra of the HSPhOH ligand alone and of the assemblies with an increasing number of HSPhOH ligand equivalents (from 0.0 eq. to 0.4 eq.). The spectra are normalized on the signal of the CO vibration at 2040 cm⁻¹. The black square represents the magnified region shown in Fig. 2g.

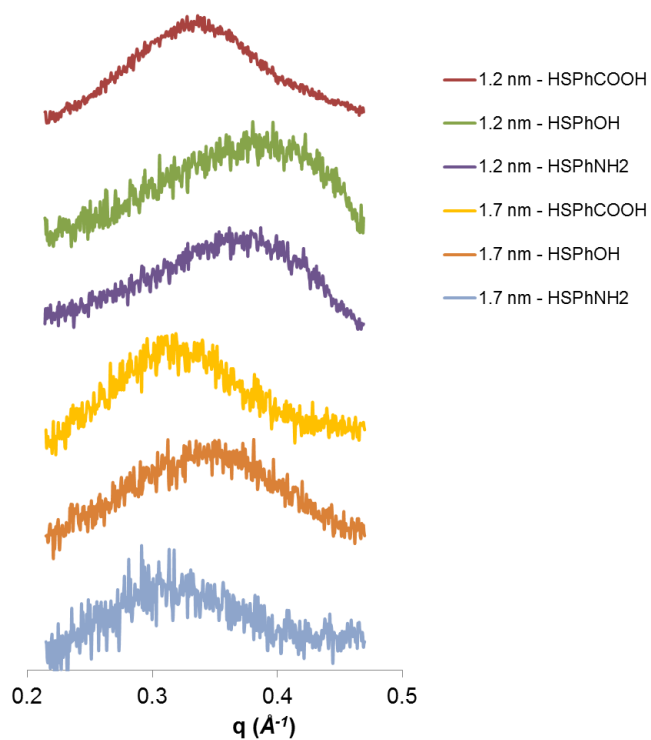


Fig. S4 Small angle X-ray scattering patterns for two series of platinum nanoparticle of different sizes (1.2 and 1.7 nm), with 0.2 eq. of different ligands (HSPhNH₂, HSPhOH, and HSPhCOOH). The correlation distances $s = 2\pi / q_{max}$ depend on the nanoparticle size (shown in Table S1).

	$d (\pm 0.05 \text{ nm})$	$s (\pm 0.05 \text{ nm})$	$\varepsilon_r (\pm 0.05)$	$Ec \text{ (eV)}$	ξ
HSPhCOOH	1.7	2.1	2.7	0.38 ± 0.04	2.74 ± 0.06
HSPhOH	1.7	1.9	5.2	0.14 ± 0.02	2.26 ± 0.05
HSPhNH ₂	1.7	2.1	7.1	0.14 ± 0.01	2.23 ± 0.06
HSPhCOOH	1.2	1.9	2.7	0.89 ± 0.10	3.40 ± 0.07
HSPhOH	1.2	1.6	5.2	0.33 ± 0.04	2.66 ± 0.06
HSPhNH ₂	1.2	1.7	7.1	0.28 ± 0.04	2.46 ± 0.05

Table S1. Nanoparticle size d , inter-particle distance s , dielectric constant of the ligands ε_r , charging energy Ec , and power exponent ξ of the six samples considered in Fig. 3f-h, Fig.4c-d and Fig. S4 (assemblies of platinum nanoparticle of different sizes – 1.2 and 1.7 nm – with 0.2 eq. of different ligands – HSPhNH₂, HSPhOH, and HSPhCOOH). d , s and ε_r are determined experimentally; Ec is calculated with the equation given in the main text; and ξ is fitted from the I - V curves.

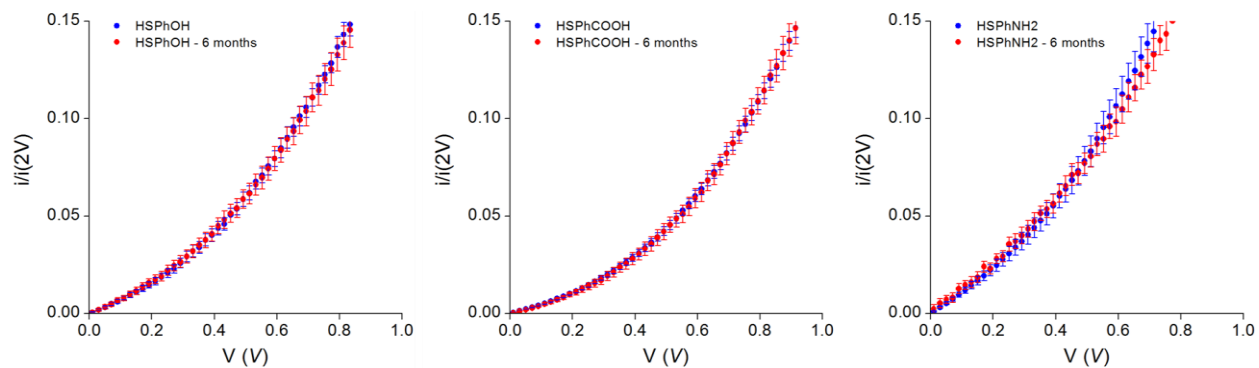


Fig. S5 Comparison of the charge transport measurements performed by conductive AFM measurements for the three samples with different ligands (HSPhNH₂, HSPhOH, and HSPhCOOH) after storing in air at room temperature for six months; zoom on the 0-1 V region, the curves are normalized at 2 V. The systems are extremely stable; no significant modification of their charge transport characteristics is noticed after six months.

	M (g.mol ⁻¹)	D (g.cm ⁻³)	n	ϵ_r	α_{CM} (bohr ³)	α_{Calc} (bohr ³)	α_{Calc_axial} (bohr ³)
HSC ₇	132	0.844	1.451	2.11	113	113	146
HSC ₈	146	0.843	1.452	2.11	125	126	164
HSC ₉	160	0.842	1.455	2.12	138	139	182
HSC ₁₀	174	0.841	1.458	2.13	152	152	200
HSC ₁₁	188	0.841	1.459	2.13	164	165	219
HSC ₁₂	202	0.845	1.459	2.13	175	177	237

Table S2. Molar mass M , density D , refractive index n , dielectric constant of the ligands ϵ_r , and polarizabilities α_{CM} , α_{Calc} , and α_{Calc_axial} of the six samples considered in Fig. 3a-d and Fig. 4a-b (assemblies of 1.3 nm platinum nanoparticle with 0.2 eq. of alkyl ligands – HSC₇ to HSC₁₂). M , D , and n are given by chemical providers; ϵ_r is deduced from n by $\epsilon_r = n^2$; α_{CM} is calculated with the Clausius-Mossotti relation $\alpha_{CM} = (\epsilon_r - 1)/(\epsilon_r - 2) * 3 M / (4 \pi D N_A)$, where N_A is the Avogadro number; α_{Calc} and α_{Calc_axial} are calculated by DFT (α_{Calc} is the global polarizability and α_{Calc_axial} is the axial polarizability along the axis of the molecules in a *trans* conformation). α_{Calc} is in very good agreement with the α_{CM} values, validating the choice of the basis for the DFT calculations. The axial polarizability α_{Calc_axial} is significantly higher than the global polarizability α_{Calc} , reflecting the anisotropy of the molecule in a *trans* conformation.

	d (± 0.05 nm)	s (± 0.05 nm)	ϵ_{r_Calc} (± 0.05)	$\epsilon_{r_Calc_axial}$ (± 0.05)	Ec (eV)	Ec_{axial} (eV)	ξ
HSC ₇	1.3	1.9	2.10	2.60	0.91 ± 0.10	0.74 ± 0.08	3.11 ± 0.07
HSC ₈	1.3	2.0	2.11	2.63	1.00 ± 0.11	0.80 ± 0.09	3.29 ± 0.06
HSC ₉	1.3	2.2	2.12	2.67	1.17 ± 0.13	0.93 ± 0.10	3.29 ± 0.06
HSC ₁₀	1.3	2.3	2.13	2.69	1.25 ± 0.14	0.99 ± 0.11	3.44 ± 0.06
HSC ₁₁	1.3	2.4	2.14	2.72	1.33 ± 0.14	1.04 ± 0.11	3.40 ± 0.08
HSC ₁₂	1.3	2.5	2.14	2.75	1.41 ± 0.15	1.10 ± 0.10	3.43 ± 0.05

Table S3. Nanoparticle size d , inter-particle distance s , dielectric constants of the ligands ϵ_{r_Calc} and $\epsilon_{r_Calc_axial}$, charging energies Ec and Ec_{axial} , and power exponent ξ of the six samples considered in Fig. 3a-d, Fig. 4a-b and Table S2 (assemblies of 1.3 nm platinum nanoparticle with 0.2 eq. of alkyl ligands – HSC₇ to HSC₁₂). d and s are determined experimentally, ϵ_{r_Calc} and $\epsilon_{r_Calc_axial}$ are obtained with the Clausius-Mossotti relation from the polarizabilities α_{Calc} et α_{Calc_axial} given in Table S2, Ec and Ec_{axial} are calculated with the equation given in the main text with ϵ_{r_Calc} and $\epsilon_{r_Calc_axial}$, respectively, and ξ is fitted from the I - V curves.

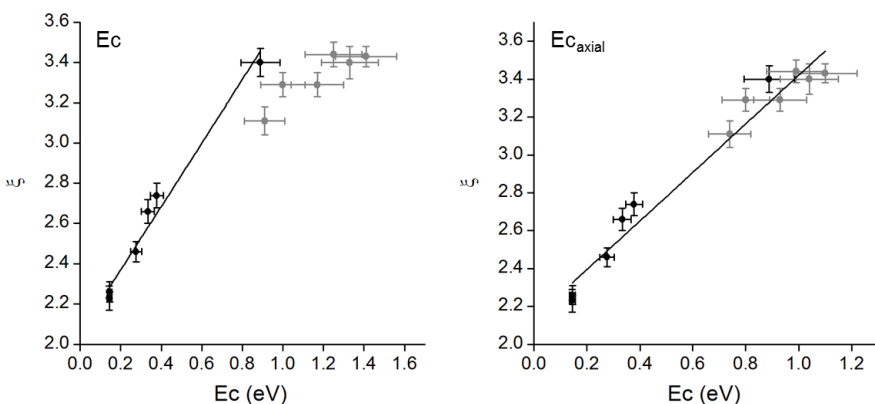


Fig. S6 Comparison of the evolution of the power exponent (fitted from the I - V characteristics showed in Figure 4c – in black, with aryl ligands, and in Figure 4b – in grey, with alkyl ligands) as a function of the charging energies (obtained from the experimental and DFT calculated parameters provided in Supplementary Tables 1,2 and 3), depending if the charging energy of the alkyl thiols is calculated with the global polarizability $\alpha_{Calc}(E_c)$, or with the axial polarizability α_{Calc_axial} along the axis of the molecules in a *trans* conformation ($E_{c_{axial}}$). The charging energies of the aryl thiols are identical in the two plots. The global behavior is linear considering the axial polarizability and not the global one. This observation suggests a charge transport through the whole backbone of the alkyl molecules, in a *trans* conformation.